

Time and Position Resolution of the Scintillator Strips for a Muon System at Future Colliders

Dmitri Denisov^a, Valery Evdokimov^b, Strahinja Lukić^{c,*}

^aFermilab, Batavia IL, USA

^bInstitute for High Energy Physics, Protvino, Russia

^cVinča Institute, University of Belgrade, Serbia

arXiv:1512.06729v3 [physics.ins-det] 29 Mar 2016

Abstract

Prototype scintillator+WLS strips with SiPM readout for a muon system at future colliders were tested for light yield, time resolution and position resolution. Depending on the configuration, light yield of up to 36 photoelectrons per muon per SiPM has been observed, as well as time resolution of 0.45 ns and position resolution along the strip of 7.7 cm.

Keywords: Linear Collider, Muon system, Scintillator, Position resolution

1. Introduction

Several concepts of future colliders, including e^+e^- colliders, are currently under study for the next generation of particle physics experiments [1, 2, 3, 4]. Due to the well-defined initial state of the interactions, low backgrounds and radiation levels, e^+e^- colliders are an attractive option for precision measurements to test various theoretical extensions of the Standard Model in the areas where the predictions of the beyond Standard Model theories differ by a few percent, such as in the Higgs sector.

The detector concepts for the future e^+e^- colliders have been developed to a high level of detail over the past decade. Since the publication of the Letters of Intent of the two major concepts, the Silicon Detector (SiD) [5] and the International Large Detector (ILD) [6], numerous technical details have been specified to an advanced level. R&D prototypes of individual subsystems reach levels of complexity involving hundreds of thousands of readout channels (See e.g. Refs. [7, 8]).

However, for the muon systems relatively few specific details are developed, and few experimental tests of detection technologies have been performed. The muon system is envisioned as several layers of position-sensitive detectors embedded in the iron flux-return yoke of the solenoidal magnet. The role of the muon system at an e^+e^- collider is primarily the identification of muons and track matching to the central tracker, besides serving as the tail catcher for the hadronic showers that penetrate beyond the hadron calorimetry. Examples of previous experimental studies dedicated to the muon-system include tests of a similar detection technique as presented here, but focusing on light yield and attenuation [9], and beam tests of a multi-layer prototype devoted to a study of the improvement of energy resolution of a hadronic calorimeter by using the muon system

as tail catcher [10]. The analogue hadronic calorimeter developed and prototyped by the CALICE collaboration uses square scintillator tiles in sizes ranging from $3 \times 3 \text{ cm}^2$ to $12 \times 12 \text{ cm}^2$ with WLS fibers and SiPM readout with the aim of reconstructing the hadronic showers with optimal energy resolution [11]. A detailed study of the detection technique similar to the one presented here, focusing on light yield and attenuation for excellent MIP detection efficiency in very long strips for long-baseline neutrino detectors is presented in Ref. [12].

The achievable precision of track matching is limited by the multiple scattering in the detector components before the muon system. The effect of the multiple scattering on track matching can be estimated using the formula by Highland [13]. The total thickness of material in the radial direction between the central tracker and the muon system corresponds to about 150-300 radiation lengths, depending on the polar angle. Muons in jets, if they have sufficient p_T to reach the muon system, typically have energies below 10 GeV. Muon spectrum in the process $e^+e^- \rightarrow Z \rightarrow q\bar{q}$ is shown in Fig. 1 as an example. At such energies, the contribution of the multiple scattering to the smearing of the muon system track position at the first muon-system layer is 5 cm or more. Tracks of higher-energy muons, such as those coming from $Z \rightarrow \mu\mu$ decay, are less disturbed by the multiple scattering. Such relatively isolated muons are, however, less challenging for track matching in comparison to muons in jets. Fig. 1 shows the example of energy distribution of muons from the Z boson decay in the Higgsstrahlung process at a 250 GeV e^+e^- collider.

The total area of the muon detectors to be instrumented with sensitive layers is several thousand square meters. Besides, the iron yoke presents an environment difficult to access for maintenance. For these reasons, economic solutions for a robust and reliable large-area detector are important.

Occupancies in the muon system are moderate at e^+e^- colliders, except in the endcap region of a CLIC collider [14]. This allows to consider a strip geometry for the sensitive layers in or

*Corresponding author

Email address: slukic@vinca.rs (Strahinja Lukić)

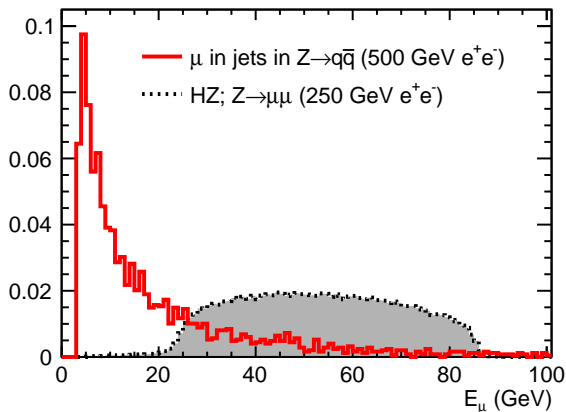


Figure 1: (Color online) Muon energy distribution for muons with sufficient p_T to reach the muon system. Solid line: muons in jets in the $e^+e^- \rightarrow Z \rightarrow q\bar{q}$ process at a 500 GeV e^+e^- collider. Dashed line: muons from the $Z \rightarrow \mu\mu$ decay in the Higgsstrahlung process at a 250 GeV e^+e^- collider.

der to limit the number of readout channels. A promising option consists of scintillator strips with WLS fibers and SiPM readout [15]. In such a system, the coordinates of the muon track are reconstructed using the observables such as the position of the strip hit by a passing muon and the signal time difference Δt between the ends of the strip to measure position along the strip. If a muon system has strip orientations alternating by 90 degrees in neighboring layers, the muon track can be reconstructed using only the positions of the strips that fired. In this case, the measurement of the position along each strip using Δt may serve to improve the precision of the track fit and to resolve “ghosts” arising at the intersections of strips hit by different particles. In the case when perpendicular orientation of strips is not feasible for access to the ends of the strips, time difference remains the only source of information on longitudinal position.

This article is the first in a series devoted to the study of the time resolution and the position resolution achievable from the time difference between the ends of scintillator strips with WLS fibers and SiPM readout. The measurements described in this paper have been performed using cosmic muons at the location of the $D\emptyset$ assembly building at the Fermi National Accelerator Laboratory, Batavia, USA, at the elevation of 220 m above sea level. The local cosmic muon fluence has been measured previously by the MicroBooNE collaboration to be $\sim 100 \text{ m}^{-2} \text{ s}^{-1}$, with a peak energy between 1 and 2 GeV [16].

Hamamatsu S10931-050P SiPMs with a sensitive area of $3 \times 3 \text{ mm}^2$ and 3600 pixels each were used for the tests [17]. Various scintillators and fibers were used as described below.

Section 2 describes the measurement setup, Sec. 3 describes the amplitude and cross-talk calibration, Sec. 4 describes the tested scintillator strip – WLS fiber configurations, Sec. 5 gives details of the data analysis, in Sec. 6 measurement results are given and the conclusions are given in Sec. 7.

2. Measurement Setup

The setup that was used for the measurements is shown in Fig. 2. It was designed to detect cosmic muons by coincidence between vertically arranged scintillation counters. S1 and S2 are plastic scintillation counters located above and below the tested strip, each of them 1 m long, 10 cm wide and 1 cm thick. S3 is a 1 cm thick scintillation counter with an area of $10 \times 15 \text{ cm}$, oriented with its 10 cm side along the tested strip located at 6 cm vertical distance from the tested strip. S4 is a 40 cm long, 2.7 cm wide and 1.2 cm thick scintillation counter oriented across the tested strip and located at 2 cm vertical distance from the tested strip. The counters S1-4 were read out using vacuum photomultiplier tubes (PMT). SiPM1 and SiPM2 denote the SiPMs connected to the respective ends of the WLS fiber of the tested strip. The length of the tested strips is 1 m.

Coincidence between S1, S2 and S3 was used as the trigger, signalling the passage of a muon. The signal from S3 was delayed by 20 ns with respect to the signals from S1 and S2, so that the trigger signal is always formed at the rising edge of the S3 signal.

The counters S3 and S4 were used to restrict the location of the muon to an area smaller than the expected position resolution of the tested strip. The location of S3 and S4 along the tested strip was changed from run to run, keeping the relative position of S3 and S4 always the same. The distance from the axis of the tested strip to the PMTs of S3 and S4 was kept constant to ensure a stable time reference for the measurement of the time resolution of the tested strip. The reason for using two counters for the location restriction was the yet unknown resolution of the tested strips. The counter S4 provided precise location at the cost of slow counting due to the small intersection area with the tested strip. The counter S3 provided better counting rate, but introduced an uncertainty of $\pm 5 \text{ cm}$ on the longitudinal position. In the offline analysis it was established that the number of hits in the intersection with the counter S4 with 7-12 hours per point was sufficient, and that the location precision provided by S4 was necessary to accurately measure the position resolution of the best tested strip. Therefore in the final analysis, the presence of the signal in S4 was required for event selection.

When measuring properties close to either end of the tested strip, the counters S1 and S2 were moved along the axis in order to cover locations up to at least 20 cm beyond the end of the tested strip. This was done in order to prevent loss of the muon flux, which would have caused a loss of statistic and a muon position bias at these points.

A CAMAC system with a LeCroy 2249A 12-input charge-sensitive ADC [18] and a LeCroy 2228A 8-input TDC [19] was used to digitize the amplitude and the arrival time of the signals. The data collection was performed and monitored from a PC with USB connection to the CAMAC Crate controller of type CC-USB by Wiener Plein&Baus, using custom-made software [20].

The signals from S4, SiPM1 and SiPM2 were recorded. Each of the signals to be recorded was first split into the time- and the amplitude detection channels using linear fan-in fan-

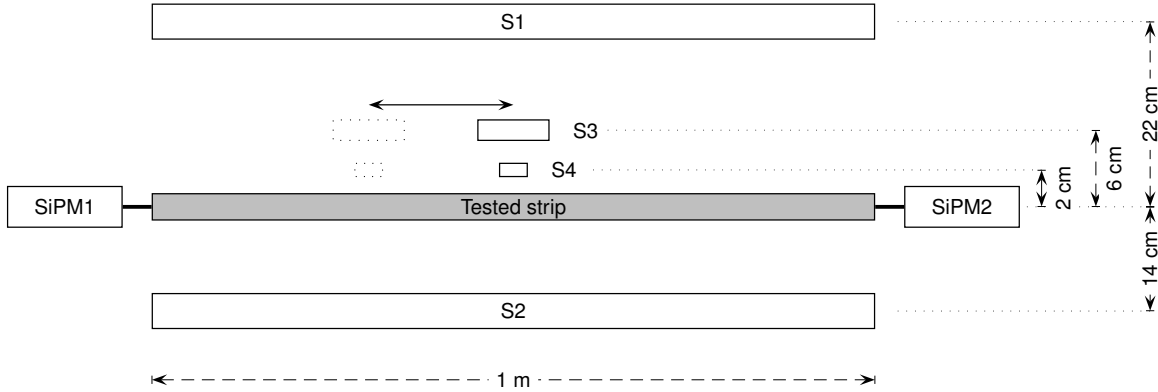


Figure 2: Schematic of the test setup. S1 and S2 are scintillation counters with vacuum PMTs positioned above and below the tested strip. S3 and S4 are small-area scintillators with vacuum PMT used to select events where the muon hits specific location along the tested strip. The location of S3 and S4 w.r.t the tested strip was changed from run to run, keeping the relative position of S3 and S4 always the same. SiPM1 and SiPM2 represent the SiPMs connected to the respective ends of the WLS fibers of the tested strip.

out modules. The time signals were processed using constant threshold discriminators. The time signals were delayed by ~ 50 ns and digitized by the TDC CAMAC module using the trigger signal as the start. The amplitude signals were delayed by ~ 40 ns and digitized by the ADC CAMAC module, using gate generated by the trigger signal.

A modified setup was used for the measurement of the light yield per muon (Sec. 4) and of the attenuation length (Sec. 5.4). In the modified setup the counters S3 and S4 were replaced by a 60 cm long, 2.7 cm wide and 1.2 cm thick *reference* strip counter parallel to the tested strip, located at a 2.5 cm vertical distance, and read out at both ends with vacuum PMTs for muon track longitudinal position measurement. The time resolution of the strip counter is similar to the S4 counter. The center of the reference strip was positioned to match the center of the tested strip. Using the reference strip we collected required statistics in a reasonable time covering a range of positions along the tested strip. A detailed description of both setups and of all performed measurements is given in Ref. [21].

The tested strips described here are shorter than what is planned for the muon system at future colliders, while facilitating the prototype studies. In longer strips the signal undergoes more attenuation. The measurement of the attenuation length is described in Sec. 5.4.

3. Photon sensitivity and cross-talk calibration

ADC scale calibration in number of photoelectrons detected was performed by illuminating SiPM with short LED pulses. The driving voltage for the LED had a triangular pulse shape. The stability of the amplitude was monitored by recording an inverted driving signal in a separate ADC channel.

Figure 3 shows an example of the measured ADC spectrum from a SiPM. The peaks in the spectrum correspond to integer numbers of pixels that fire. When the light intensity is low the *pedestal* peak, corresponding to the events in which no pixels

have fired, is clearly visible. The center of the pedestal peak, representing the zero signal, and the average distance between the centers of the neighboring peaks, representing the single pixel signal amplitude, are used to express the signal amplitude in terms of the number of pixels that have fired, n_{pixel} .

Each detected photon may cause 1 or more pixels to fire. The ratio of the average number of fired pixels, $\langle n_{pixel} \rangle$, to the average number of detected photons, ν , at low light intensity is generally larger than 1 due to the optical and electrical cross-talks, as well as the afterpulsing (see [22]). For simplicity we combine all these effects under the common *cross-talk factor* $X = \langle n_{pixel} \rangle / \nu$.

The probability for detecting zero photons is $P_0 = e^{-\nu}$. P_0 is measured as the ratio of the number of events in the pedestal peak, A_0 , to the integral of the whole spectrum, A , allowing to extract the average number of detected photons as $\nu = -\ln(A_0/A)$. On the other hand, the average number of fired pixels is determined from the mean of the measured spectrum. Thus the cross-talk factor is obtained as,

$$X = -\frac{\langle n_{pixel} \rangle}{\ln(A_0/A)} \quad (1)$$

The cross-talk factor depends on several parameters, including the bias voltage applied to the SiPM and its temperature. The bias voltage was kept constant to within 0.1 V for the duration of the tests. The experimental room was climatized, limiting the temperature variations. During the tests, the value of the cross-talk factor was measured several times, and the results were centered around $X = 1.35$ with relative variations within $\pm 5\%$.

4. Tested configurations

Four configurations of the scintillator strip with WLS fibers were tested for the light yield. The light yields given here refer

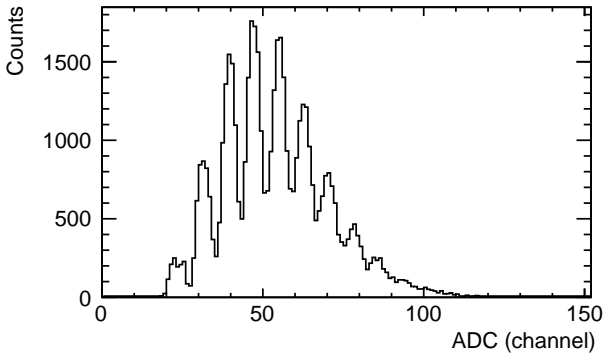


Figure 3: ADC spectrum of a SiPM illuminated by LED pulses.

to the average number of detected photons per cosmic-ray muon hit. The position of muon hits was distributed in the region of ± 30 cm from the center of the tested strip (see description of the modified setup in Sec. 2).

The four configurations, denoted *A*, *B*, *C* and *D*, are schematically presented in Fig. 4. The description of the used strips, fibers and light insulation follows:

Scintillator strips

Configurations *A* and *C* were built with clear polystyrene scintillator strips with a 40×10 mm² profile, co-extruded with a TiO₂ loaded surface layer such as used by the MINOS collaboration [23]. Configurations *B* and *D* were built with clear Bicon[®] 404A fast scintillator strip with a 27×12 mm² profile [24].

WLS fibers

Configurations *A* and *B* used polystyrene double-clad fibers of 1.2 mm diameter with 175 ppm of Y-11 fluor produced by Kuraray Inc. Japan. One such fiber was inserted into the groove and covered with white Tyvek[®] sheet type 1056D [25, 26] in configuration *A*, while seven fibers were attached to the narrower side of the strip using reflective adhesive tape in 5 points along the strip in configuration *B*. Configurations *C* and *D* used Bicon[®] BCF-92 WLS fibers of 1.0 mm diameter. Four fibers were inserted into the groove of the strip in configuration *C* and covered with the Tyvek[®] sheet, while in configuration *D* seven fibers were attached to the narrower side of the strip using reflective adhesive tape. Configurations *B* and *D* were additionally wrapped with one layer of the Tyvek[®] sheet, and all configurations were finally wrapped in several layers of black Tedlar[®] paper [25, 26].

In configurations using seven fibers, the ends of the fibers extended 20 cm beyond the end of the strip and were bundled together so that six fibers surrounded one in a tight hexagonal shape. In the configuration using 4 fibers, the fibers were bundled in an approximately square form. In this way it was possible to efficiently collect light from the fibers onto the 3×3 mm² area of the SiPMs. No optical glues or greases were used for the connection of the fibers to the scintillator strips or to the SiPMs.

Configurations *B* and *D* were designed based on the experience from the upgrade of the DØ muon system [27].

The measured light yield per muon was 10, 19, 20 and over 30 photoelectrons on each end of the strip in configurations *A*, *B*, *C* and *D*, respectively. The configurations *C* and *D* were selected for detailed position- and time-resolution studies.

5. Data Analysis

5.1. Event selection

The off-line event selection was performed as follows:

1. Events in which either of the S4, SiPM1 or SiPM2 signals is below the discriminator threshold, signalled by the end-of-scale value in the respective TDC channel, were rejected.
2. Events with energy deposit in the S4 counter below 75% of the most probable energy deposit were rejected.

5.2. Longitudinal position resolution and the speed of signal propagation along the strip

The location of the muon impact was defined by the position x of the S4 counter along the axis of the tested strip. The center of the tested strip was assigned the relative position $x = 0$, and the x axis was oriented away from SiPM2 towards SiPM1. Five points along the strip were measured for the configurations *C* and *D*. The data for each point were collected over 7 to 12 hours in order to collect the statistics of at least 500 events remaining per point after the selection cuts.

The observable with the best sensitivity to muon position along the strip is the time difference between the two SiPMs. Position is thus measured as,

$$x_{SiPM} = b_0 + v^* \frac{t_{SiPM2} - t_{SiPM1}}{2} = b_0 + v^* \frac{\Delta t}{2} \quad (2)$$

where b_0 is the offset and v^* is the speed of the signal propagation along the tested strip.

The time of the rising edge detection by the constant threshold discriminator depends on a signal amplitude. Beside worsening the time resolution, this effect also introduces a position-dependent bias especially at the strip ends due to a difference in SiPM signals caused by different attenuation in the opposite directions.

The amplitude effect was corrected by subtracting the amplitude-dependent delay of the form $\delta t = a_1/A$, where A is the amplitude of the signal. To obtain the parameter a_1 , the function $t = a_0 + a_1/A$ was fitted to the scatter plot of the time versus amplitude for both SiPMs separately at $x = 0$, i.e. when S4 is at the center of the tested strip (Fig. 5). The parameter a_0 is the constant time offset of the SiPM in the high-amplitude limit.¹

The speed of the signal propagation along the strip is determined from the linear fit to the plot of x vs. $\langle \Delta t/2 \rangle$ in the five

¹Correction of the amplitude effect for the S4 counter, although in principle relevant, was not necessary due to the fast signal and high amplitude in the counter for the selected events.

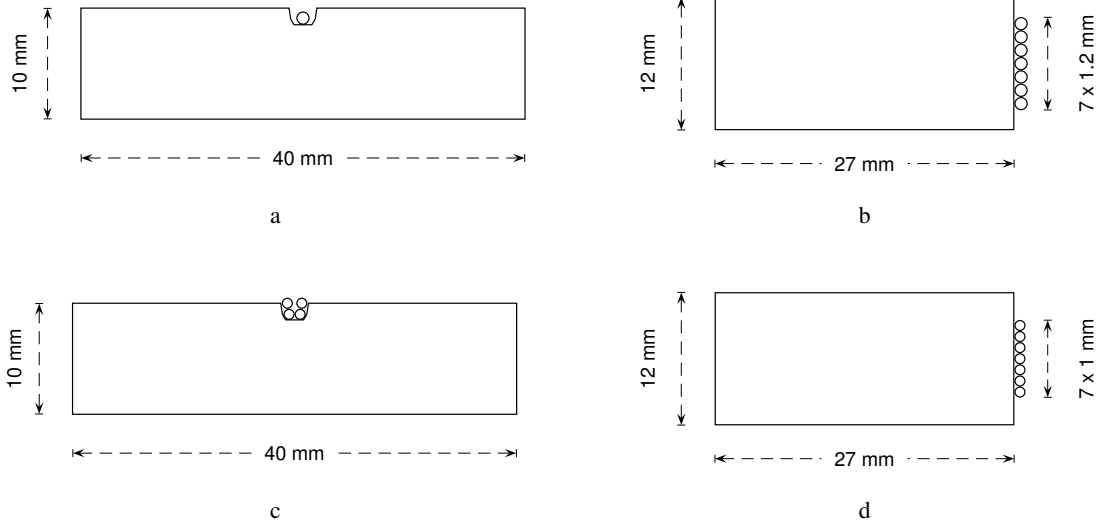


Figure 4: Tested configurations of the scintillator strip with WLS fibers: **a** configuration A – MINOS strip with one Kuraray WLS fiber, **b** configuration B – Bicorn strip with 7 Kuraray WLS fibers, **c** configuration C – MINOS strip with 4 Bicorn WLS fibers, **d** configuration D – Bicorn strip with 7 Bicorn WLS fibers.

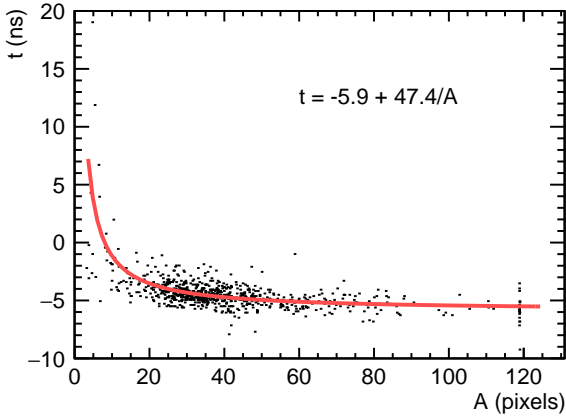


Figure 5: (Color online) Scatter plot of time vs. amplitude of SiPM1 from the dataset taken at the S4 position $x = 0$ with configuration D, showing the amplitude-dependent delay of the timing signal from the discriminator. The function used for the correction of this effect is also shown (continuous line).

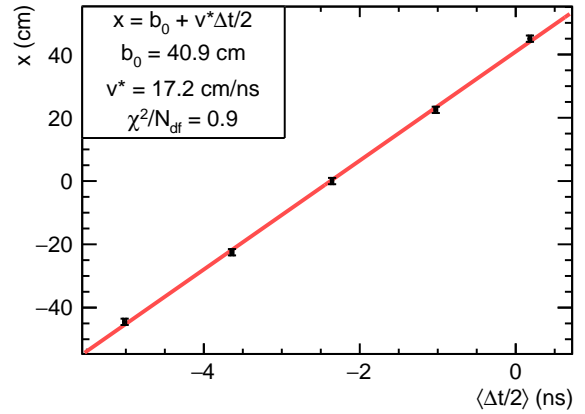


Figure 6: (Color online) Plot of x vs. $\frac{\Delta t}{2}$ for the configuration D. Linear fit is also shown.

measured points, as shown in Fig. 6. The uncertainty on $\Delta t/2$ was estimated from the scatter of the data, while the uncertainty on x was set to 1 cm, corresponding to the estimated precision of the position of the S4 counter.

The distribution of the variable $\Delta t/2$ after the amplitude correction (Fig. 5) is shown in Fig. 7 for the configuration D and $x = 0$. The standard deviation of the distribution, determined from a Gaussian fit, is the crucial parameter for the counter position resolution. The average value of the standard deviation of $\Delta t/2$ from all 5 measured points in configuration D was $\sigma_{\Delta t/2} = 0.45$ ns.

The position resolution along the strip can be estimated as $\sigma_x = \sigma_{\Delta t/2} v^* = 7.7$ cm for the configuration D. Beside the po-

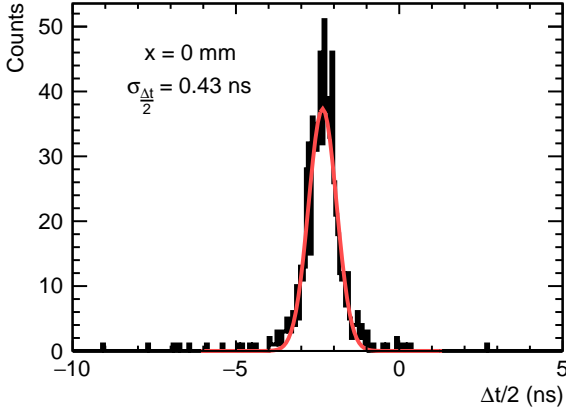


Figure 7: (Color online) Distribution of $\Delta t/2$ after the amplitude correction for the configuration D and $x = 0$. Gaussian fit is also shown.

sition resolution of the tested strip, this estimate contains contributions from the uncertainty of the muon impact position along the tested strip due to the width of the S4 counter and the uncertainty due to the angular distribution of the muon tracks across the distance between S4 and the tested strip. This estimate of the coordinate resolution along the tested counter can thus be regarded as conservative.

5.3. Time resolution

The most direct way to measure strip time resolution is to analyze the distribution of the average time of the two SiPMs at the ends of the tested strip $(t_1 + t_2)/2$. As the average time of the tested strip does not depend on the position of S4 along the tested strip within measurement uncertainty, the data from all 5 studied S4 positions are added up. The distribution of average times is shown in Fig. 8 for the configuration D . The standard deviation of the fitted Gaussian curve is 0.52 ns. The dominant contribution to the width of the distribution is the time resolution of the tested strip, but other contributions are also present, such as the time resolution of S4. Also, the width of the tested strip introduces a spread in the muon positions w.r.t. the PMT of S4.

Another estimate of the time resolution of the tested strip can be inferred from $\sigma_{\Delta t/2}$. Since amplitude effect on t_1 and t_2 is corrected as shown in Fig. 5, the statistical fluctuations of t_1 and t_2 are independent of each other and the variance of $\Delta t/2 = (t_1 - t_2)/2$ is the same as that of $(t_1 + t_2)/2$. The average value of $\sigma_{\Delta t/2}$ for the 5 measured points in configuration D is 0.45 ns. The time resolution of S4 does not contribute to $\sigma_{\Delta t/2}$. Nevertheless, contributions from uncertainties other than the time resolution of the tested strip are still present, such as the uncertainty of the muon- position due to the width of S4 counter.

The time resolution of both SiPM channels individually was determined as the average Gaussian width of the distribution of $t_{\text{SiPM}} - t_{\text{S4}}$ in all five measured points. In configuration D the result is $\sigma_{t, \text{SiPM1}} = 0.68$ ns and $\sigma_{t, \text{SiPM2}} = 0.63$ ns.

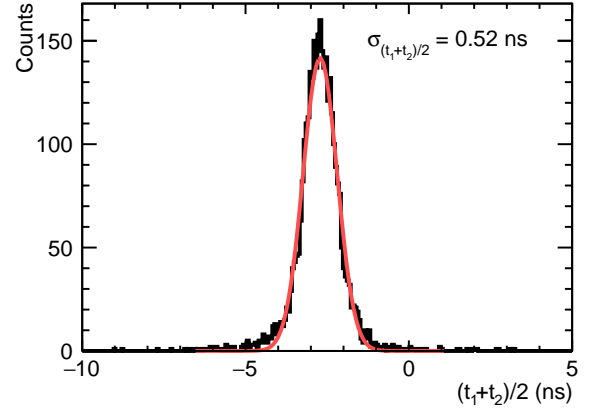


Figure 8: (Color online) Distribution of the average times for the strip configuration D w.r.t. S4. Gaussian fit is also shown.

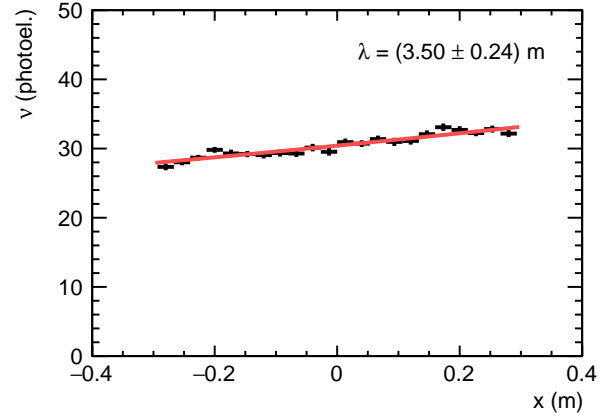


Figure 9: (Color online) Plot of the mean value of the SiPM1 photon count vs. muon position in configuration D . Fit of the exponential function and the attenuation length are also shown.

5.4. Attenuation of light along the strip

Attenuation of the light signal along the tested strip was measured in the modified setup described in Sec. 2.

Figure 9 shows a plot of the mean value of SiPM1 photon count in configuration D vs. muon position. Exponential fit to the data indicates an attenuation length for the light signal in this strip of $\lambda = 3.5 \pm 0.2$ m. This value is consistent with the statement of the manufacturer of the WLS fibers that $\lambda \geq 3.5$ m [28].

The observed attenuation length of the tested strips is smaller than the expected size of the muon system. Increase in both the attenuation length and the light yield will be beneficial for the muon system design.

6. Results

Table 1 summarizes the measured performance of the individual SiPM readout channels for the configurations C and D .

Table 1: Measured performance of the individual SiPM readout channels for the configurations *C* and *D*.

Configuration	SiPM #	Light yield / muon (photoelectrons)	$\sigma_{t,\text{SiPM}}$ (ns)
<i>C</i>	1	21	1.2
	2	20	1.1
<i>D</i>	1	31	0.68
	2	36	0.63

Table 2: Measured properties of the strip configurations *C* and *D*.

Configuration	σ_x (cm)	$\sigma_{t,\text{strip}}$ (ns)	v^* (cm/ns)	λ (m)
<i>C</i>	16.0	0.88	18.1	2.1
<i>D</i>	7.7	0.45	17.2	3.5

The average number of photoelectrons per muon is sufficiently high to ensure a 100 % detection efficiency for muons traversing the entire thickness of the strip. Time resolution per readout channel of the order of 1 ns or better was achieved with signals of only 20 to 30 photoelectrons on average.

Table 2 summarizes the results of the strip studies including position and time resolutions, signal propagation speed and the attenuation length. The difference in the resolutions for the two configurations is larger than the ratio expected if the resolution follows the $1/\sqrt{\nu}$ law, where ν is the number of photons. This indicates that other factors besides the statistical effect of the photon yield influence the time and the position resolutions. These additional effects include the properties of the scintillator and the WLS fiber materials, especially the light emission time.

The best measured position resolution in the studies described here is 7.7 cm, achieved with the configuration *D*.

7. Conclusions

Prototype scintillator+WLS strip configurations with SiPM readout for a muon system for the future colliders were tested for light yield, position resolution and time resolution. Depending on the configuration, a light yield in single SiPM of up to 36 photoelectrons per muon has been achieved. Strip time resolution of 0.45 ns and position resolution of 7.7 cm were achieved. Tests with higher statistics more precise timing and muon position reference, such as in the test-beam, will yield results with better accuracy.

A muon system for future colliders based on scintillator strips with WLS fibers and SiPM readout would possess excellent muon-detection efficiency, a time resolution suitable even for challenging beam time structure such as that of the CLIC design, and a position resolution sufficient for track matching with the central detector for the broad range of physics processes. The attenuation length of the WLS fibers limits the acceptable strip length. In the endcap region of a CLIC collider, the occupancy from muon beam halo background also presents a constraint on the strip length [14]. The reliability of operation,

the economy of production and the relatively low required number of readout channels make this technology a very attractive option.

8. Acknowledgments

The authors acknowledge the support received from the Ministry of Education and Science and the National Research Center ‘‘Kurchatov Institute’’ (Russian Federation), from the Ministry of Education, Science and Technological Development (Republic of Serbia) within the project OI171012 and from the Department of Energy (United States of America).

References

- [1] ILC Collaboration, *The International Linear Collider - Technical Design Report*, 2013, ILC-REPORT-2013-040. URL <http://www.linearcollider.org/ILC/TDR>
- [2] CLIC Collaboration, *Compact linear collider – Conceptual Design Report*, 2012. URL <http://clic-study.web.cern.ch/content/conceptual-design-report>
- [3] M. Benedikt, F. Zimmermann, *Towards Future Circular Colliders*, 2015, CERN-ACC-2016-004. URL <http://cds.cern.ch/record/2120669/>
- [4] The CEPC-SPPC Study Group, *CEPC-SppC Preliminary Conceptual Design Report*, 2015, IHEP-CEPC-DR-2015-01. URL <http://cepc.ihep.ac.cn/preCDR/volume.html>
- [5] H. Aihara, P. Burrows, M. Oreglia (Eds.), SiD Letter of Intent, no. SLAC-R-989 – FERMILAB-LOI-2009-01 – FERMILAB-PUB-09-681-E, 2009, arXiv:0911.0006.
- [6] ILD Concept Group, *The International Large Detector – Letter of Intent*, Report DESY 2009/87 – Fermilab PUB-09-682-E – KEK Report 2009-6 (2010). URL <http://ilcild.org/>
- [7] J. Repond, Recent DHCAL Developments, in: International Workshop on Future Linear Colliders (LCWS13) Tokyo, Japan, 11-15 November 2013, 2013, arXiv:1312.3868.
- [8] V. Buridon, et al., First results of the CALICE SDHCAL technological prototype, arXiv:1602.02276 (2016).
- [9] V. Balagura, M. Danilov, B. Dolgoshein, S. Klemin, R. Mizuk, P. Pakhlov, E. Popova, V. Rusinov, E. Tarkovsky, I. Tikhomirov, *Study of scintillator strip with wavelength shifting fiber and silicon photomultiplier*, Nuclear Instruments and Methods in Physics Research Section A: Accelerators, Spectrometers, Detectors and Associated Equipment 564 (1) (2006) 590 – 596. doi:<http://dx.doi.org/10.1016/j.nima.2006.04.030>. URL <http://www.sciencedirect.com/science/article/pii/S0168900206006413>
- [10] C. Adloff, et al., Construction and performance of a silicon photomultiplier/extruded scintillator tail-catcher and muon-tracker, *Journal of Instrumentation* 7 (04) (2012) P04015. URL <http://stacks.iop.org/1748-0221/7/i=04/a=P04015>
- [11] The CALICE collaboration, *Construction and commissioning of the CALICE analog hadron calorimeter prototype*, *Journal of Instrumentation* 5 (05) (2010) P05004. URL <http://stacks.iop.org/1748-0221/5/i=05/a=P05004>
- [12] O. Mineev, Y. Kudenko, Y. Musienko, I. Polyansky, N. Yershov, *Scintillator detectors with long WLS fibers and multi-pixel photodiodes*, *Journal of Instrumentation* 6 (12) (2011) P12004. URL <http://stacks.iop.org/1748-0221/6/i=12/a=P12004>
- [13] V. L. Highland, *Some practical remarks on multiple scattering*, *Nuclear Instruments and Methods* 129 (2) (1975) 497 – 499. doi:[http://dx.doi.org/10.1016/0029-554X\(75\)90743-0](http://dx.doi.org/10.1016/0029-554X(75)90743-0). URL <http://www.sciencedirect.com/science/article/pii/0029554X75907430>
- [14] E. van der Kraaij, B. Schmidt, *Muon system design studies for detectors at CLIC*, Note LCD-Note-2011-008, CERN (2011). URL <http://cds.cern.ch/record/1443353>

- [15] T. Behnke, et al. (Eds.), *The International Linear Collider - Technical Design Report*, Vol. 4: Detectors, International Linear Collider, 2013, ILC-REPORT-2013-040, arXiv:1306.6329.
URL <http://www.linearcollider.org/ILC/TDR>
- [16] K. Woodruff, et al., *Studies of the Cosmic Ray Flux in MicroBooNE*, in: APS April Meeting April 5–8, 2014, Savannah, Georgia, 2014.
URL http://www-microboone.fnal.gov/talks/APSApril_woodruff.pdf
- [17] *Hamamatsu News*, January 2009 (Web document accessed December 2015).
URL https://www.hamamatsu.com/sp/hpe/HamamatsuNews/HamamatsuNews_0109.pdf
- [18] *LeCroy Models 2249A, 2249W, 2249SG and 2259B CAMAC Analog-to-Digital Converters* (Web document accessed December 2015).
URL <http://teledynelecroy.com/lrs/dsheets/2249.htm>
- [19] *LeCroy Models 2228A, 2229 and 4208 CAMAC Time-to-Digital Converters* (Web document accessed December 2015).
URL <http://teledynelecroy.com/lrs/dsheets/2228.htm>
- [20] S. Lukić, *Wiener-DAQ program for data acquisition with Wiener CC-USB CAMAC Controller* (Web document accessed December 2015).
URL <http://vinhep.vin.bg.ac.rs/strahinja-software/SiPM/WienerDAQdocu.pdf>
- [21] D. Denisov, V. Evdokimov, S. Lukić, *Tests of scintillator+WLS strips for muon system at future colliders*, arXiv:1510.03030 (2015).
- [22] B. Dolgoshein, et al., *Status report on silicon photomultiplier development and its applications*, Nucl. Inst. Meth. A 563 (2) (2006) 368 – 376.
URL <http://www.sciencedirect.com/science/article/pii/S0168900206004578>
- [23] The MINOS Collaboration, *The magnetized steel and scintillator calorimeters of the MINOS experiment*, Nucl. Inst. Meth. A 596 (2008) 190–228. doi:10.1016/j.nima.2008.08.003.
- [24] *Saint Gobain Crystals – Premium plastic scintillators; data sheet* (Web document accessed December 2015).
URL <http://www.crystals.saint-gobain.com/uploadedFiles/SG-Crystals/Documents/SGC%20BC400-404-408-412-416%20Data%20Sheet.pdf>
- [25] *E. I. du Pont de Nemours* (Web site accessed December 2015).
URL <http://www.dupont.com>
- [26] V. Abazov, et al., *The muon system of the run II DØ detector*, Nuclear Instruments and Methods in Physics Research Section A: Accelerators, Spectrometers, Detectors and Associated Equipment 552 (3) (2005) 372 – 398. doi:<http://dx.doi.org/10.1016/j.nima.2005.07.008>.
URL <http://www.sciencedirect.com/science/article/pii/S0168900205014105>
- [27] V. Evdokimov, *Light collection from scintillation counters using WLS fibers and bars*, AIP Conf. Proc. 450 (1998) 300. doi:10.1063/1.56976.
- [28] *Saint Gobain Crystals – Scintillating optical fibers brochure* (Web document accessed December 2015).
URL <http://www.crystals.saint-gobain.com/uploadedFiles/SG-Crystals/Documents/SGC%20Fibers%20Brochure.pdf>